



RESEARCH ARTICLE OPEN ACCESS

Quantitative Iron Measurements in the Basal Ganglia of NBIA Patients Using QSM: Insights From a Tertiary Center

Özge Uygun¹  | Alpay Özcan²  | Fuat Kaan Aras³ | Evrim Bozdemir⁴ | Sibel Uğur İşeri⁵ | Koray Kırımtay⁶ | Arzu Karabay⁶ | Murat Gültekin⁷ | Nihan Hande Akçakaya⁸ | Orkhan Mammadov⁹ | Gülay Kır¹⁰ | Dilek İnce Günel¹¹ | Neşe Tuncer¹² | Fatma Betül Özdilek¹³ | Banu Özen Barut¹⁴ | Ercan Köse¹⁵ | Hülya Apaydın¹ | Asuman Ali¹⁶ | Sultan Çağırıcı¹⁷ | Pınar Topaloğlu¹⁸ | Alp Dinçer¹⁹ | Zuhul Yapıcı¹⁸

¹Department of Neurology, Cerrahpasa Faculty of Medicine, İstanbul University-Cerrahpasa, İstanbul, Turkey | ²Electrical and Electronics Engineering Department, Bogazici University, İstanbul, Turkey | ³Department of Neuropathology, Institute of Pathology, University Hospital Heidelberg, Heidelberg, Germany | ⁴Department of Anesthesiology and Reanimation, Acibadem Altunizade Hospital, Acibadem Mehmet Aydınlar University Faculty of Medicine, İstanbul, Turkey | ⁵Department of Genetics, Aziz Sancar Institute of Experimental Medicine, İstanbul University, İstanbul, Turkey | ⁶Department of Molecular Biology and Genetics, İstanbul Technical University, İstanbul, Turkey | ⁷Department of Neurology, Erciyes University School of Medicine, Kayseri, Turkey | ⁸Department of Neurology, Faculty of Medicine, Demiroglu Bilim University, İstanbul, Turkey | ⁹Department of Anesthesiology and Reanimation, İstanbul Medical Park Hospital, İstanbul, Turkey | ¹⁰Department of Anesthesiology and Reanimation, Faculty of Medicine, Koc University, İstanbul, Turkey | ¹¹Department of Neurology, Marmara University Pendik Training and Research Hospital, İstanbul, Turkey | ¹²Department of Neurology, Acibadem Mehmet Aydınlar University Faculty of Medicine, Acibadem Altunizade Hospital, İstanbul, Turkey | ¹³Department of Neurology, İstanbul Medeniyet University Goztepe Training and Research Hospital, İstanbul, Turkey | ¹⁴Department of Neurology, Kartal Training and Research Hospital, İstanbul, Turkey | ¹⁵Department of Neurology, SBU Gulhane Training and Research Hospital, Ankara, Turkey | ¹⁶Department of Neurology, Bursa Yuksek İhtisas Training and Research Hospital, Bursa, Turkey | ¹⁷Department of Neurology, Bakirkoy Dr. Sadi Konuk Training and Research Hospital, İstanbul, Turkey | ¹⁸Department of Neurology, İstanbul University, İstanbul Faculty of Medicine, İstanbul, Turkey | ¹⁹Department of Radiology, Faculty of Medicine, Acibadem Mehmet Ali Aydınlar University, İstanbul, Turkey

Correspondence: Özge Uygun (uygunoz01@gmail.com)

Received: 27 February 2025 | **Revised:** 14 June 2025 | **Accepted:** 30 June 2025

Funding: The authors received no specific funding for this work.

Keywords: basal ganglia | iron accumulation | Kufor Rakeb syndrome | MPAN | MRI | NBIA | PKAN | PLAN | QSM

ABSTRACT

Objective: Neurodegeneration with brain iron accumulation (NBIA) comprises rare genetic disorders characterized by predominantly extrapyramidal symptoms and iron deposition in the basal ganglia. Conventional magnetic resonance imaging (MRI) detects qualitative changes but cannot accurately quantify iron accumulation. Quantitative susceptibility mapping (QSM) allows precise in vivo quantification of iron, providing insight into the pathophysiology of the disease.

Methods: We studied 27 genetically confirmed NBIA patients and 11 age-matched healthy controls using susceptibility-weighted imaging (SWI) on a 3 Tesla MRI scanner. Basal ganglia regions of interest (ROIs) were manually delineated and QSM values were extracted.

Results: Sixteen NBIA patients and 11 controls were analyzed. QSM showed significantly higher iron in the globus pallidus (GP) ($p=0.008$), with PKAN patients showing a 2.5-fold increase in GP iron ($p=0.001$). MPAN patients showed 2.5 times higher iron

[Correction added on 6 October 2025, after first online publication: Koray Kırımtay and Arzu Karabay has been added to the author list.]

Abbreviations: BFMRS, The Burke Fahn Marsten dystonia scale; BPAN, Beta-propeller protein-associated neurodegeneration; BW, bandwidth; GP, globus pallidus; MPAN, mitochondrial membrane protein-associated neurodegeneration; MRI, magnetic resonance imaging; NC, nucleus caudatus; P, putamen; PKAN, pantothenate kinase-associated neurodegeneration; PLAN, *PLA2G6*-associated neurodegeneration; QSM, quantitative susceptibility mapping; ROI, regions of interest; SN, substantia nigra; SWI, susceptibility-weighted imaging; TE, echo time; TH, thalamus; TR, repetition time.

This is an open access article under the terms of the [Creative Commons Attribution-NonCommercial-NoDerivs](https://creativecommons.org/licenses/by-nc-nd/4.0/) License, which permits use and distribution in any medium, provided the original work is properly cited, the use is non-commercial and no modifications or adaptations are made.

© 2025 The Author(s). *Annals of Clinical and Translational Neurology* published by Wiley Periodicals LLC on behalf of American Neurological Association.

in both GP and substantia nigra (SN). A GP iron level >0.1133 ppm increased the likelihood of PKAN 18-fold. Atypical PKAN cases had 2.5 times higher SN iron levels compared to classic cases.

Interpretation: QSM is a sensitive and noninvasive tool for detecting and quantifying iron accumulation in NBIA. The GP consistently showed the highest susceptibility values across subtypes, emphasizing its significant role in disease pathology. Distinct patterns of iron deposition in different NBIA subtypes may reflect subtype-specific mechanisms with diagnostic and therapeutic relevance. Age-related susceptibility changes were found to be significant, reinforcing the need to account for age when interpreting QSM data. More importantly, QSM may serve as a candidate biomarker for longitudinal disease monitoring in future clinical trials targeting disease-modifying therapies in NBIA.

1 | Introduction

Neurodegeneration with brain iron accumulation (NBIA) comprises a heterogeneous group of genetic disorders characterized by progressive neurological deterioration, predominantly extrapyramidal symptoms, and pathological iron deposition in the basal ganglia [1]. Clinically, these disorders manifest with dystonia, parkinsonism, spasticity, and cognitive decline, often leading to severe disability and premature mortality. Genetic mutations underlying NBIA disturb iron homeostasis in the brain, resulting in iron accumulation as a key neuropathological feature. The estimated prevalence of NBIA is approximately 1 to 3 cases per million, with at least 15 distinct subtypes identified to date [2]. Given the rarity of these disorders and their broad phenotypic spectrum, accurate diagnosis and disease monitoring remain a significant clinical challenge.

Most NBIA disorders follow an autosomal recessive inheritance pattern, with the exception of one autosomal dominant and one X-linked dominant subtype. Certain NBIA subtypes also exhibit mitochondrial dysfunction, either directly or through metabolic pathways such as CoA synthesis, fatty acid hydroxylation, myelin synthesis, and autophagy, resulting in a broad spectrum of age at onset and clinical presentations [3]. This genetic and biochemical heterogeneity underlies a wide range of clinical manifestations, including variability in age at onset, symptom severity, and radiological findings. Since the identification of *PANK2*, the gene responsible for pantothenate kinase-associated neurodegeneration (PKAN), research has led to the sequential discovery of additional genetic variants underlying other NBIA subtypes. These include *PLA2G6*-associated neurodegeneration (PLAN) in 2006, mitochondrial membrane protein-associated neurodegeneration (MPAN) in 2011, and beta-propeller protein-associated neurodegeneration (BPAN) in 2012, each associated with distinct defective proteins and disease mechanisms [4–8]. More recently, Kolorova et al. [2] proposed that additional genetic mutations contributing to basal ganglia iron accumulation may also be classified under the NBIA spectrum. Despite advances in gene discovery, the relationship between specific genotypes and the regional distribution of iron deposition remains incompletely understood, particularly in atypical presentations.

Magnetic resonance imaging (MRI) is crucial for diagnosing NBIA disorders, primarily by detecting iron deposition. In most NBIA disorders, iron accumulation is evident on MRI at the time of diagnosis. For example, the “eye of the tiger” sign observed on T2-weighted images is a characteristic MRI feature useful for diagnosing PKAN [9]. In conditions such as MPAN, iron accumulation predominantly occurs in the globus pallidus (GP) and substantia

nigra (SN). Identification of a striatal line on T2-weighted images in the pallidum can prompt clinicians to consider C19orf12 mutation analysis to confirm an MPAN diagnosis [10]. For BPAN, a hyperintense halo in the SN on T1-weighted MRI images is a distinctive feature. In aceruloplasminemia, iron accumulation extending beyond the basal ganglia, combined with markedly reduced ceruloplasmin levels and elevated ferritin levels, are key diagnostic indicators. While these NBIA subtypes present with distinct MRI patterns that can suggest specific genetic mutations, the majority lack pathognomonic features, and conventional sequences may not detect early or subtle iron accumulation, especially in atypical or late-onset cases. Quantitative susceptibility mapping (QSM), a recent MRI method, has emerged as a valuable tool for detecting brain iron in its early stages, even when iron is not yet visible with standard MRI. QSM provides critical insights into disease progression by quantifying iron deposition in specific brain regions [11, 12].

The primary aim of this study was to quantitatively assess iron accumulation in the basal ganglia of NBIA patients using QSM, and to explore specific patterns of iron distribution across NBIA subtypes, particularly between atypical and classic PKAN phenotypes. Unlike earlier studies, our research provides novel insights by quantitatively comparing iron levels in key basal ganglia regions, including the GP, SN, putamen (P), and caudate nucleus (NC), across clinically and genetically distinct NBIA subgroups. Furthermore, the study aimed to investigate whether QSM-derived iron metrics could serve as potential diagnostic markers to differentiate PKAN from other NBIA subtypes and from healthy controls. This included evaluating a cut-off value using receiver operating characteristic (ROC) analysis. By addressing both anatomical distribution and phenotypic heterogeneity, this study aims to bridge the gap between genotype, imaging, and clinical expression in NBIA.

2 | Methods

2.1 | Subjects

This study included 41 patients with a genetically confirmed diagnosis of NBIA between 1999 and 2019 at Istanbul University, Istanbul Faculty of Medicine, Department of Child Neurology. Among these, six patients had undergone deep brain stimulation, and eight had deceased, leaving 27 eligible patients who underwent MRI scans using the relevant QSM protocol. For comparison, 11 healthy controls matched for age and gender were included. These individuals had no prior neurological disorders, motor or cognitive impairments, chronic medication use,

traumatic brain injury, or family history of neurodegenerative diseases. The classification into classic and atypical PKAN was based on clinical presentation: Classic forms showed early onset, generalized dystonia with rapid progression, while atypical cases were marked by slower evolution, parkinsonism, and predominant speech involvement [1–5]. All patients underwent periodic neurological examinations, and dystonia severity was assessed using the Burke-Fahn-Marsden Dystonia Rating Scale (BFMRS), which ranges from 0 to 120. The study was approved by the Local Ethics Committee (2017/658), and written informed consent was obtained from all participants or their legal guardians.

2.2 | MRI Data Collection

This institutional review board (IRB)-approved study included 16 NBIA patients who successfully completed the MRI protocol, of whom 11 underwent imaging under anesthesia. The patient group consisted of 9 individuals with PKAN (7 males and 2 females), 2 with PLAN (both male), 3 with MPAN (all male), and 2 with Kufor-Rakeb syndrome (1 male and 1 female). The mean age of the patient cohort was 21.37 ± 13.98 years (range: 5–35 years), except for one 56-year-old PKAN patient. Additionally, 11 healthy controls (5 females, mean age: 29.54 ± 13.76 years, range: 7–49 years) underwent MRI scans using the same protocol without anesthesia. Prior to imaging, written informed consent was obtained from all participants or their legal representatives.

2.3 | MRI Acquisition

MRI data were acquired using a Siemens Magnetom Prisma 3T scanner, equipped with a 60 cm gantry, 80 mT/m gradients (200 T/m/s slew rate), and a 64-channel head/neck coil. For QSM analysis, a 3D FLASH sequence was utilized with the following parameters: echo time (TE) = 30 ms, repetition time (TR) = 45 ms, resolution = $0.86 \times 0.86 \times 2$ mm per voxel, and matrix size = 256×256 . Axial images were obtained for further analysis. MRI data were processed using a standardized pipeline. First, all images were converted from DICOM to NIfTI format using the MIPAV (Medical Image Processing, Analysis, and Visualization) software. Brain surface extraction (BSE) was performed using the BSE algorithm in MIPAV to generate masks for subsequent analysis [13].

For QSM reconstruction, raw phase images were processed using the STI Suite v2.2 software, following a series of preprocessing steps: phase scaling to 2π , phase unwrapping, and background phase removal using the iHARPERELLA algorithm (integrated Harmonic Background Phase Removal using the Laplacian operator) [14–16]. Final susceptibility maps were generated using the iLSQR (improved sparse linear equation and least-squares) algorithm [17].

Regions of interest (ROIs) in the basal ganglia, including the NC, P, GP, red nucleus (RN), and SN, were manually segmented. ROIs were delineated in 2D on axial slices corresponding to the largest cross-sectional area of each nucleus. Initial segmentation was performed independently on unprocessed phase images or frequency shift maps using the polygon drawing tool in MIPAV by an experienced researcher (FKA, > 5 years of experience).

To ensure anatomical precision and intersubject consistency, the delineation process was conducted in collaboration with a neurologist specialized in movement disorders and a professor of biomedical engineering with expertise in neuroimaging analysis. Subsequently, all segmented ROIs were reviewed and verified for anatomical accuracy by a senior radiologist with extensive experience in neuroradiology. Inter-rater reliability metrics were not computed due to the centralized and consensus-based segmentation process. Mean QSM values within each ROI were extracted using in-house MATLAB 2018b (MathWorks, Natick, MA, USA) scripts [17]. Negative susceptibility values, arising from diamagnetic interference or phase-processing artifacts, were excluded from analysis to prevent distortion of QSM-based iron quantification.

2.4 | Statistical Analysis

All statistical analyses were performed using SPSS 26 (SPSS Inc., Chicago, IL, USA). A 95% confidence interval (CI) was applied, and statistical significance was set at $p < 0.05$. The distribution of variables was assessed using visual (histogram) and analytical methods (Kolmogorov–Smirnov & Shapiro–Wilk tests). Group comparisons were conducted using Student's *t*-test for parametric data and the Mann–Whitney U test for nonparametric data. Correlations between imaging findings and clinical variables were assessed using Spearman's rank correlation coefficient. ROC analysis was performed to determine potential cut-off values for basal ganglia iron accumulation. In addition, logistic regression analysis was used to evaluate the predictive utility of QSM-derived iron measurements in distinguishing NBIA patients from healthy controls. To account for the potential confounding effect of age on susceptibility values, correlation analyses (Spearman's rho) and multiple linear regressions including age, sex, and disease duration as predictors were performed for each ROI.

3 | Results

3.1 | Subject Characteristics

Among the 41 genetically confirmed NBIA patients initially evaluated, 27 underwent QSM analysis following MRI. However, due to processing errors, QSM data from 11 patients were excluded. The final analysis included 16 NBIA patients and 11 age- and sex-matched healthy controls (six males, 55%; five females, 45%). The mean age of the patients was 22.69 ± 14.01 years (range: 5–56 years), with a mean age of disease onset of 11.5 ± 10.6 years (range: 2–24 years). The cohort consisted of 9 PKAN, 3 MPAN, 2 PLAN, and 2 KRS patients, with a mean follow-up period of 2.56 ± 2.13 years (range: 1–9 years). Consanguineous marriage was reported in 44% of the patients ($n = 12$). Genetic and clinical characteristics are presented in Table 1.

Among the 9 PKAN patients, five exhibited classic PKAN, whereas four had atypical features. In the classic PKAN group, mutation analysis revealed one missense mutation, one splice donor mutation, one frameshift mutation, and one patient with both a stop-gain and a missense mutation. While

TABLE 1 | Clinical characteristics and genetics of NBIA patients.

Clinical diagnosis	Patient ID	CA	OA	Variant and zygosity	Variant effect	Initial symptoms	FH	PS	EPS	BFMS (0–120)	Follow-up (year)	Other findings
PKAN patients												
Typical	Classical PKAN	28	4	PANK2 (hom): ENST00000316562.9:c.655G>A: p.(Gly219Ser)	Missense	Night blindness	+	–	Blepharospasm Axial and distal extremity dystonia+++ Parkinsonism+	108	3	Irritability, impulsivity
Typical	Classical PKAN	10	2	PANK2 (hom): ENST00000316562.9:c.628+2T>G	Splice donor	Walking difficulty	+	+	Generalized dystonia+++	120	2	Retinitis pigmentosa
Typical	Classical PKAN	7	3	PANK2 (comp het): ENST00000316562.9:c.494_495delG C; (p.Arg165Profs*15) and c.1426_1429delATGA; p.(Met476Alafs*18)	Frameshift	Walking difficulty and balance problems	–	+	Generalized dystonia+++ Postural instability++	76	3	Retinitis pigmentosa
Typical	Classical PKAN	5	5	PANK2 (comp het): ENST00000316562.9:c.1351C>T; p.(Arg451Ter) and c.1466 T> C; p.(Leu489Pro)	Stop gained and missense	None	+	–	–	0	1	Retinitis pigmentosa
Typical	Classical PKAN	7	2	PANK2 (comp het): ENST00000316562.9:c.1351C>T; p.(Arg451Ter) and c.1466 T> C; p.(Leu489Pro)	Stop gained and missense	Speech problem and walking difficulty	+	+	Generalized dystonia+++	98	1	Retinitis pigmentosa
Atypical	Atypical PKAN	37	24	PANK2 (comp het): ENST00000316562.9:c.1133A>G; p.(Asp378Gly) and c.1412G>A, p.(Ser471Asn)	Missense and missense at splice region	Speech problem and walking difficulty	–	+	Blepharospasm and distal limb dystonia Tachylalia Parkinsonism++ Postural instability+++	40.5	2	
Atypical	Atypical PKAN	26	19	PANK2 (hom); ENST00000316562.9:c.800A>C; p.(His267Pro)	Missense	Speech and balance problems	–	–	Tachylalia Parkinsonism+ Postural instability+++	10	5	
Atypical	Atypical PKAN	56	23	PANK2 (hom); ENST00000316562.9:c.1583C>T; p.Thr528Met	Missense	Speech problem and walking difficulty	–	+	Tongue and lower extremity dystonia++ Parkinsonism++ Postural instability+	48	1	

(Continues)

TABLE 1 | (Continued)

Clinical diagnosis	Patient ID	CA	OA	Variant and zygosity	Variant effect	Initial symptoms	FH	PS	EPS	BFMS (0–120)	Follow-up (year)	Other findings
Atypical PKAN		30	19	PANK2 (hom); ENST00000316562.9: c.401A > G (p.Glu134Gly)	Missense	Night blindness, speech problem, and walking difficulty	–	+	Limb dystonia+ Tremor+++ Rigidity++	48	1	
PLAN patients												
	PLAN	24	8	PLA2G6 (hom): ENST00000332509.8: c.2239C > T; p.Arg747Trp	Missense	Speech and behavioral problems Tremulousness	–	+	Dystonia+ Tremor +++ Rigidity++	80	9	Cognitive impairment
	PLAN	6	4	PLA2G6 (hom): ENST00000332509.8: c.2251G > A; p.Glu751Lys	Missense	Loss of motor and mental functions	–	+	Rigidity in upper extremities+ (other than flask tetraparesis)	86	1	Cognitive impairment
MPAN patients												
	MPAN	23	9	c19orf12 (hom) ENST00000323670.14: c.172G > A; p.Gly58Arg	Missense	Walking difficulty	–	+	Distal limb dystonia++ Parkinsonism++	69	4	Cognitive impairment, motor neuropathy
	MPAN	24	9	c19orf12 (hom) ENST00000323670.14:c.161-2A > G	Splice acceptor	Walking difficulty	–	+	Generalized dystonia+++ Parkinsonism++	84	1	Cognitive impairment, optic atrophy
	MPAN	16	16	c19orf12 (hom) ENST00000323670.14: c.-2C > T	5'UTR	No	+	–	–	0	1	
KRS patients												
	KRS	38	10	ATP13A2 (hom): ENST00000452699.5:c.1407_1413delins CTCCAAA: p.(Ala470Phefs*46)	Frameshift	Speech problem, poor school performance	+	SP++	Oromandibular and distal limb dystonia+ Parkinsonism+++	106	3	Cognitive impairment, Sensorial and motor neuropathy
	KRS	26	16	ATP13A (hom): ENST00000452699.5:c.1407_1413delins CTCCAAA: p.(Ala470Phefs*46)	Frameshift	Right handed tremor	+	+	Oromandibular dystonia+ Parkinsonism+++	45	3	Alopecia

Abbreviations: CA, current age; Comp Het, compound heterozygous; EPS, extrapyramidal signs; FH, family history; Hom, homozygous; OA, age at onset; PS, pyramidal signs; SP, spastic paraparesis.

patients with splice donor and missense mutations were homozygous, the remaining three classic PKAN patients carried compound heterozygous mutations. Dystonia was the predominant symptom in all classic PKAN cases. Patients with atypical PKAN demonstrated a higher frequency of missense and homozygous mutations. The BFMS score for all symptomatic classic PKAN patients was ≥ 76 , whereas for atypical PKAN patients, it was ≤ 48 . The clinical and genetic characteristics of PKAN, MPAN, PLAN, and KRS patients are summarized in Table 1.

3.2 | Quantitative Susceptibility Mapping (QSM) Results

QSM analysis was performed across all ROIs (GP, NC, P, TH, and SN). Negative results were excluded from statistical analysis, as they were likely due to interference from other metals (e.g., calcium), which affect the diamagnetic properties of the tissue and prevent accurate algorithm convergence. Mean values for each nucleus were then compared between groups (Figure 1).

3.2.1 | Age-Related Effects on Iron Accumulation

Correlation and regression analyses were performed to assess the impact of age on susceptibility values. In the overall cohort, age showed significant positive correlations with QSM values in the P ($\rho = 0.55$, $p = 0.003$), thalamus (TH) ($\rho = 0.52$, $p = 0.005$) and RN ($\rho = 0.70$, $p < 0.001$), though not in the NC or GP. Within the NBIA group ($n = 16$), age correlated significantly with QSM values in the TH ($r = 0.684$, $p = 0.003$), RN ($r = 0.735$, $p = 0.001$), and SN ($r = 0.624$, $p = 0.010$). No significant associations were found for the caudate, P, or GP. Multiple linear regression analysis showed that age was an independent predictor of QSM values in the SN ($\beta = 0.0078$, $p = 0.011$), GP ($\beta = 0.0069$, $p = 0.011$) and RN ($\beta = 0.0023$, $p = 0.023$). Sex and disease duration had no significant effects.

3.2.2 | QSM-Based Differentiation of NBIA Subtypes

Analysis revealed that iron accumulation in the GP and SN, the two nuclei showing pronounced hypointensity on conventional MRI, was approximately 2.5 times higher in NBIA patients compared to healthy controls. Specifically, iron content in the GP was significantly higher in NBIA patients than in controls ($p = 0.008$) (Figure 2). Conversely, putaminal iron levels were significantly higher in healthy controls than in NBIA patients ($p = 0.015$) (Figure 2).

In PKAN patients, GP iron levels were 2.5 times higher than in healthy controls ($p = 0.001$) (Figure 3). ROC analysis identified a cut-off value of 0.1133 ppm in the GP, above which the likelihood of a PKAN diagnosis increased 18-fold. This threshold demonstrated 75% sensitivity and 82% specificity in distinguishing PKAN patients from healthy controls (95% confidence interval).

Iron levels in the NC were significantly higher in healthy controls compared to PKAN patients ($p = 0.026$) (Figure 3). However, among PKAN patients, compound heterozygous carriers exhibited four times higher iron accumulation in the NC compared to homozygous PKAN patients ($p = 0.036$) (Figure 4).

Interestingly, iron levels in the P were lower in all NBIA patients compared to controls, and both the NC and P demonstrated reduced iron accumulation in PKAN patients relative to healthy controls. When comparing atypical ($n = 4$) and classic ($n = 5$) PKAN patients, atypical PKAN cases exhibited approximately 2.5 times higher iron accumulation in the SN ($p = 0.024$) (Figure 4). No significant differences in iron accumulation in other basal ganglia nuclei were observed between atypical and classic PKAN patients.

Compared to both healthy controls and PKAN patients, MPAN patients exhibited approximately 2.5 times greater iron accumulation in the GP ($p = 0.005$) and SN ($p = 0.036$) (Figure 5). However, no significant difference in basal ganglia iron levels was detected between PKAN and MPAN patients.

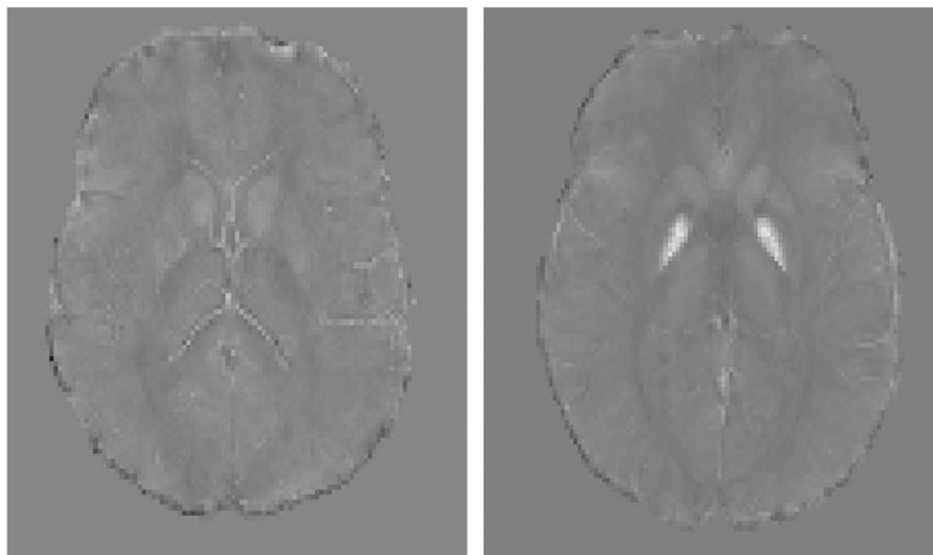


FIGURE 1 | Comparison of QSM of the basal ganglia of healthy control and PKAN patient.

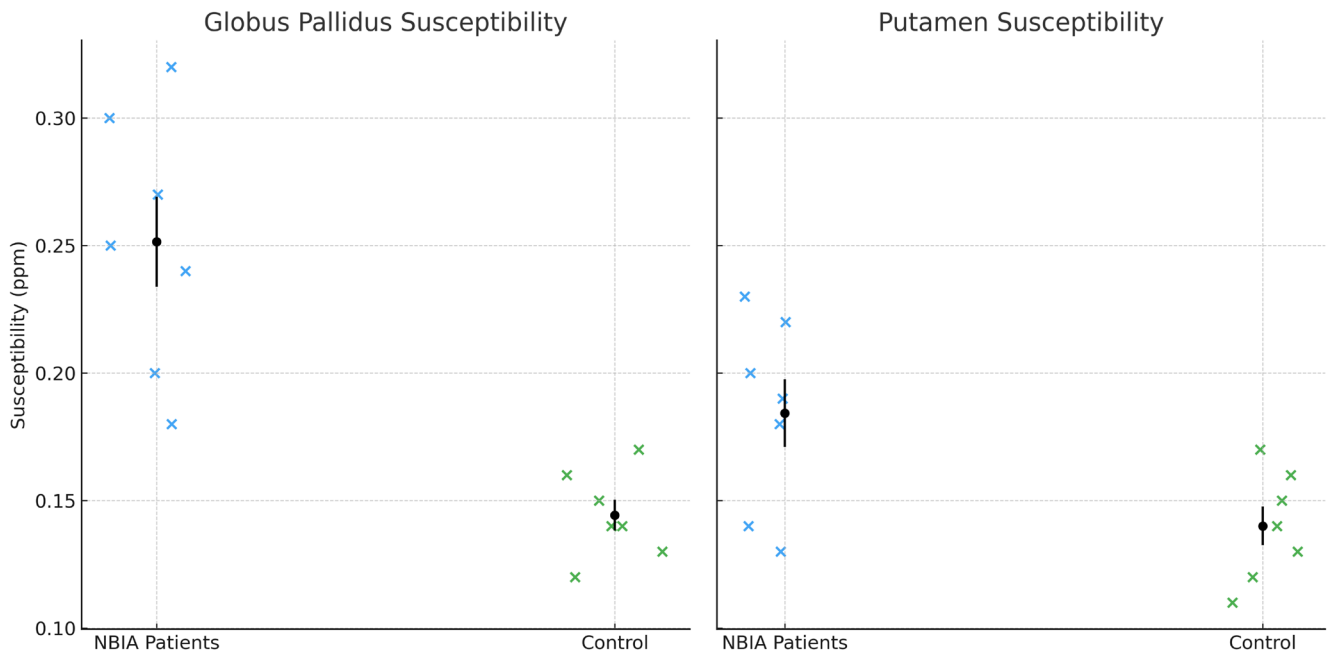


FIGURE 2 | Quantitative comparison of iron levels in (A) globus pallidus and (B) putamen nuclei between NBIA patients and healthy controls. Susceptibility values are expressed in parts per million (ppm). Statistical significance, GP ($p=0.008$), Putamen ($p=0.015$).

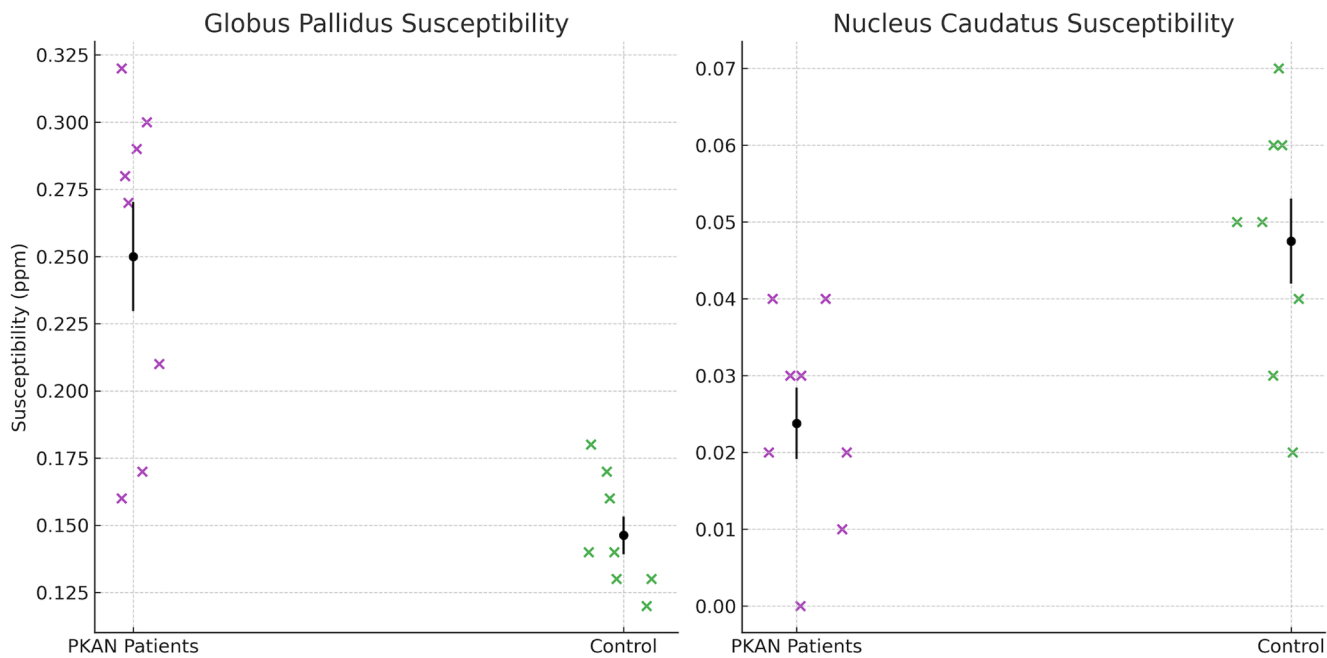


FIGURE 3 | Quantitative comparison of iron levels in (A) globus pallidus and (B) nucleus caudatus between PKAN patients and healthy controls. Susceptibility values are expressed in parts per million (ppm). Statistical significance, GP ($p=0.001$), NC ($p=0.026$).

In our cohort, only two patients each were enrolled in the PLAN and KRS groups. Although QSM demonstrated elevated iron levels in these patients compared to healthy controls, the small sample size precluded statistical analysis.

4 | Discussion

Iron is a crucial element for neuronal metabolism, particularly within mitochondrial pathways [18–24]. However, excessive

accumulation of free iron can lead to oxidative stress, lipid peroxidation, and ultimately neuronal damage. Iron accumulation in deep gray matter has been associated with motor and cognitive dysfunction, particularly in aging populations [25]. With the growing recognition of the role of iron metabolism in neurodegenerative processes, recent advances in MRI now allow for the precise visualization and quantification of iron deposition in progressive neurological disorders [26]. Iron exhibits paramagnetic properties, leading to hyperintense signals in T1-weighted MRI and hypointense signals in T2-weighted sequences [25, 27].

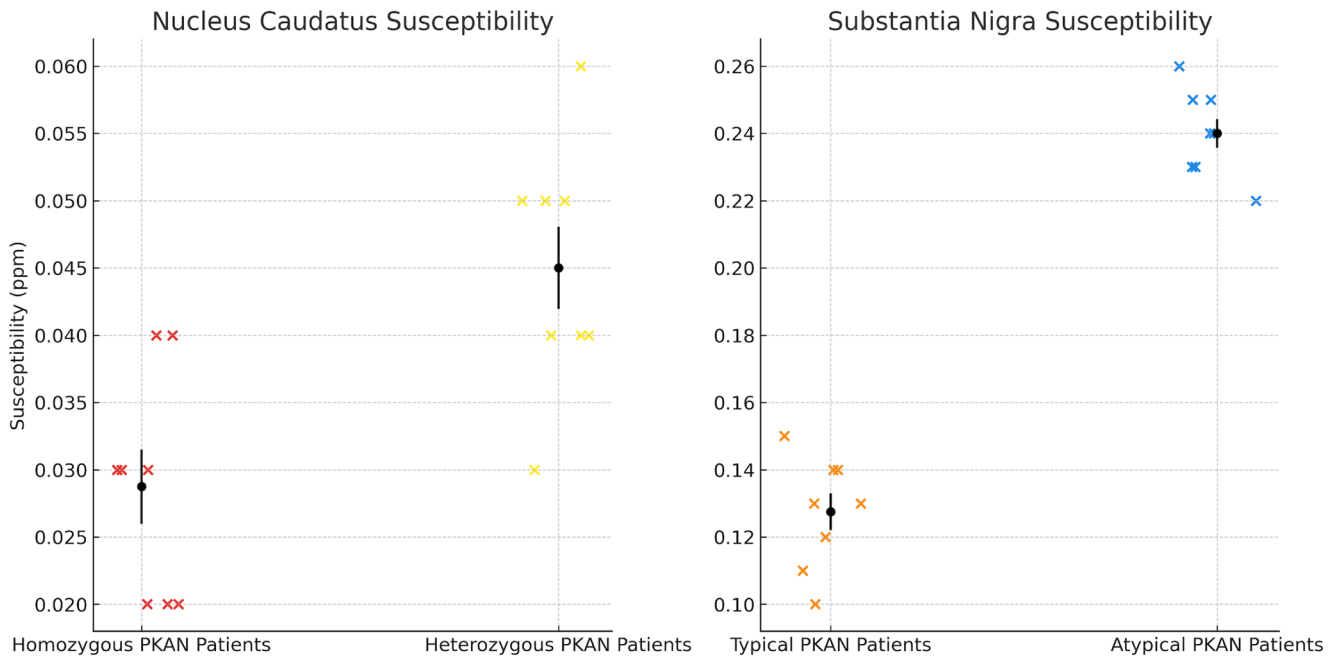


FIGURE 4 | Quantitative comparison of iron levels in (A) nucleus caudatus between patients with homozygous and heterozygous mutations and (B) substantia nigra between typical and atypical PKAN patients. Susceptibility values are expressed in parts per million (ppm). Statistical significance, NC ($p=0.036$), SN ($p=0.024$).

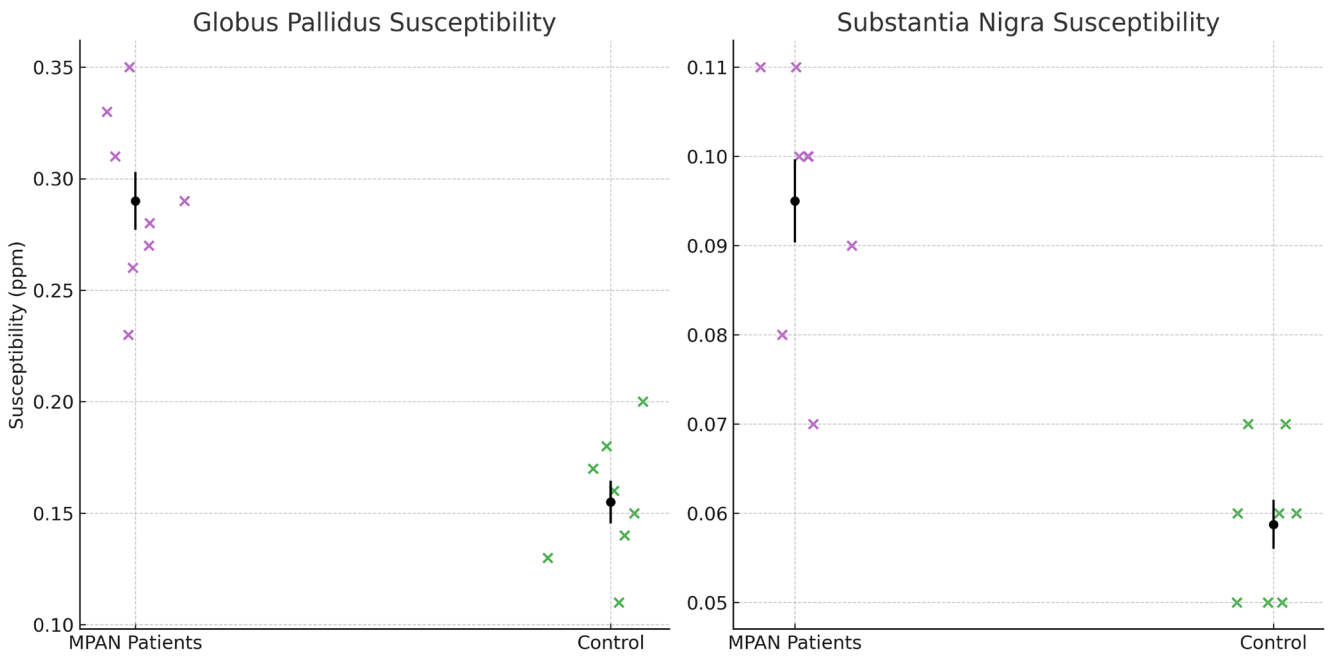


FIGURE 5 | Quantitative comparison of iron levels in (A) globus pallidus and (B) substantia nigra between MPAN patients and healthy controls. Susceptibility values are expressed in parts per million (ppm). Statistical significance, GP ($p=0.005$), SN ($p=0.036$).

Susceptibility-weighted imaging (SWI) leverages the paramagnetic properties of deoxyhemoglobin, methemoglobin, hemosiderin, and iron, providing enhanced contrast compared to conventional MRI sequences [28, 29]. SWI has proven useful in diagnosing hemorrhagic disorders, vascular malformations, hypoxic/anoxic injuries, and neurodegenerative diseases [30]. However, QSM has emerged as the most sensitive technique for iron quantification in neural tissues [31–34]. Unlike SWI,

which provides qualitative contrast, QSM quantitatively maps tissue magnetic susceptibility, making it a superior tool for differentiating myelin and iron content in the brain [35]. Given that iron dysregulation is not only a hallmark of NBIA disorders but also implicated in multiple sclerosis, Alzheimer’s disease, and Parkinson’s disease, the ability to accurately assess iron distribution with QSM becomes critical for understanding neurodegeneration and disease progression [36–40].

Dusek et al. [41] previously reported that QSM measurements in two PKAN patients and one heterozygous PANK2 mutation carrier revealed no significant iron accumulation in the heterozygous carrier, while PKAN patients exhibited approximately three times higher iron levels in the GP, SN, and internal capsule compared to controls. Our study demonstrated that iron accumulation in the GP was significantly higher in NBIA patients than in healthy controls, with an overall two-fold increase (Figure 2). This underscores the clinical relevance of GP iron load across NBIA subtypes, particularly in PKAN, where GP involvement is most pronounced. Among the nine PKAN patients included in our study, the mean iron levels were 0.2154 ppm in GP and 0.1514 ppm in SN, compared to 0.096 ppm and 0.050 ppm, respectively, in healthy controls. These values indicate that GP iron accumulation is approximately 2.5 times higher in PKAN patients than in controls (Figure 3). ROC analysis indicated that an iron level above 0.1133 ppm in the GP predicts PKAN with high specificity and sensitivity (95% CI). However, this diagnostic threshold should be interpreted with caution, given the small size of the control sample and the exploratory nature of the analysis. Similarly, the multivariate regression results should be viewed as preliminary as the current sample size may not provide sufficient statistical power for robust modeling (see Section 4.1).

Dystonia and parkinsonism are key clinical features in NBIA disorders, though their severity and distribution vary. In our PKAN cohort, classic PKAN was associated with severe dystonia, while atypical PKAN presented with milder dystonia, more pronounced parkinsonism, and slower disease progression. QSM data revealed that atypical PKAN patients exhibited significantly higher iron accumulation in the SN than classical PKAN patients (2.5-fold increase, $p=0.024$, Figure 4). These findings suggest that while GP involvement is predominant in classical PKAN, SN pathology may play a more critical role in atypical PKAN. Although our data do not establish a direct link between pallidal iron and dystonia or SN iron and parkinsonism, future studies should explore whether QSM-based iron quantification in these ROIs correlates with specific motor phenotypes. Additionally, the finding that higher SN iron accumulation is associated with atypical PKAN raises the possibility that these patients may have a milder disease course compared to classical PKAN cases. This may suggest a differing pathophysiological mechanism underlying parkinsonism-predominant forms of PKAN, potentially reflecting selective nigral vulnerability. This hypothesis warrants further investigation in larger follow-up studies, particularly in assessing treatment responses.

Cognitive impairment is a well-recognized feature in NBIA disorders, either in early or late disease stages. Several studies have highlighted the significance of iron dysregulation in cognitive decline, particularly in Alzheimer's disease and mild cognitive impairment (MCI) [37]. In one study, QSM analysis of the amygdala, hippocampus, precuneus, pulvinar nucleus, and TH provided valuable insights into iron-related neurodegeneration in MCI and Alzheimer's disease [37]. Specifically, iron accumulation in the precuneus and allocortex was found to be a distinguishing factor between MCI and normal aging. In our study, iron levels were significantly lower in the P across all NBIA patients and were also lower in both the P and NC in PKAN patients compared to healthy controls ($p=0.026$, Figure 3).

The NC plays a crucial role in cognitive function, and prior research has suggested that iron accumulation in the striatum is associated with working memory deficits in aging [42, 43]. Interestingly, contrary to aging studies, a positive correlation between caudate iron levels and working memory performance has been found in younger populations [42]. Given that striatal iron accumulation typically plateaus around age 40 [44], further research should investigate whether early iron dysregulation in the NC contributes to cognitive impairment in NBIA patients. While our study did not directly assess cognitive function, the observed reduction in caudate and putamen iron levels, contrary to age-related accumulation patterns, raises questions about the relationship between regional iron depletion and NBIA-related cognitive symptoms. However, it is important to note that in PKAN, the most prevalent NBIA subtype, cognitive function is typically preserved, at least in the early stages of the disease. This clinical observation should be taken into account when interpreting the potential link between altered iron distribution and cognitive involvement.

On the contrary, our findings demonstrate that brain iron accumulation, as reflected by QSM values, is significantly influenced by age in specific deep gray matter regions. In particular, we observed robust positive correlations between age and QSM values in the RN, TH, and SN in both the entire cohort and the NBIA patient group. These results are consistent with previous studies showing age-related increases in magnetic susceptibility in subcortical nuclei involved in motor control and basal ganglia circuits [1, 5]. Furthermore, multiple linear regression analyses confirmed that age was an independent predictor of susceptibility values in the SN, GP, and RN, whereas sex and disease duration were not significant contributors. These findings suggest that age may confound QSM measurements in neurodegeneration studies and emphasize the importance of accounting for age-related effects in future analyses. Notably, the absence of a significant age effect in certain regions (e.g., the caudate nucleus) could indicate region-specific iron dynamics or varying disease susceptibility. Overall, our data support the inclusion of age as a covariate in QSM dataset analyses and emphasize the importance of interpreting susceptibility changes within the broader context of neurodevelopmental and neurodegenerative trajectories. While our findings demonstrate significantly elevated iron levels in NBIA patients compared to healthy controls, it is important to note that age was also positively correlated with QSM values in multiple deep brain regions. Therefore, age may act as a confounding factor influencing the observed group differences. While regression analyses suggested that age was an independent predictor of susceptibility in certain regions, the possibility remains that the higher QSM values in the NBIA group may be partially attributed to age-related susceptibility changes rather than disease-specific iron accumulation. This alternative explanation should be considered when interpreting the results, and future studies should employ age-matched control groups or longitudinal designs to better isolate disease-related QSM changes.

In MPAN, pathological iron accumulation is most prominent in the GP and SN, and these regions have been the primary focus in therapeutic studies evaluating individual response to iron chelation therapy. For example, Löbel et al. [45] reported a marked reduction in SN iron levels on QSM in a 13-year-old

MPAN patient treated with deferiprone, although this radiological improvement was not accompanied by measurable clinical benefit. In our cohort ($n = 3$), mean iron levels were 0.2265 ppm in the GP and 0.115 ppm in the SN, corresponding to a 2.5-fold increase compared to healthy controls. Although such findings reinforce the utility of QSM in detecting iron overload, the clinical relevance of regional iron reduction remains uncertain. It is still unclear whether decreasing iron levels in specific nuclei translate into meaningful symptomatic relief. Therefore, future research should not only aim to quantify radiological changes but also establish clinically validated thresholds of response. Serial QSM monitoring, when integrated with functional and clinical outcomes, may ultimately serve as a more reliable biomarker for evaluating treatment efficacy in NBIA patients. In other NBIA subtypes such as PLAN, BPAN, and KRS, conventional MRI often fails to detect iron accumulation in the early stages of the disease. This limitation is particularly evident in pediatric patients, where disease progression may outpace radiological findings. QSM, however, provides a more sensitive means of detecting iron deposition, potentially identifying changes even when conventional MRI findings remain unremarkable [46–48].

Although based on a small cohort, our observations raise important considerations regarding iron homeostasis and pathological features in NBIA disorders. By integrating detailed genotype–phenotype correlations, our findings aim to offer preliminary insights into how specific genetic mutations, clinical severity, and atypical presentations may relate to regional patterns of iron accumulation. This approach may allow for a more nuanced interpretation of iron deposition beyond simple group-level comparisons and may help uncover intra-subtype variability and the diagnostic complexity of NBIA syndromes. Although our findings do not conclusively establish this, they underscore the importance of generating preliminary data in this relatively unexplored area.

While QSM offers robust anatomical and quantitative insight into iron deposition, it does not directly elucidate the underlying biological mechanisms contributing to iron dysregulation. The consistent finding of the GP as the nucleus with the highest iron accumulation across all NBIA subtypes suggests that GP iron levels may serve as a primary clinical marker. Future studies should explore longitudinal QSM measurements to determine the temporal relationship of iron accumulation between the GP and SN, and its impact on disease progression. To address the current limitations, future research should aim to integrate QSM imaging data with transcriptome-wide analyses of the brain. Combining advanced neuroimaging with molecular profiling approaches may help identify gene expression patterns and pathways involved in abnormal brain iron metabolism in NBIA. Such integrative translational studies could not only enhance our understanding of disease pathophysiology and genotype–phenotype associations but also support the development of novel therapeutic targets.

4.1 | Limitations

This study has several limitations that warrant consideration. The small sample size may limit the statistical power of

multivariate and diagnostic analyses. In particular, while the ROC curve analysis yielded a potentially useful threshold in the GP to distinguish NBIA patients from controls, this cutoff should be considered preliminary due to the limited number of control subjects. Therefore, findings from regression and ROC analyses should be interpreted with caution. Future studies with larger and more diverse control populations are needed to validate these findings, assess inter-rater reproducibility, and refine diagnostic thresholds.

Another limitation is the absence of formal inter-rater reliability testing for ROI delineation, despite the fact that all ROIs were carefully reviewed and cross-validated by experts in neurology, neuroimaging, and neuroradiology.

The relatively small number of healthy control subjects may reduce the generalizability of the findings. However, our primary aim was not to establish normative reference values, but to assess the clinical utility of QSM in a genetically confirmed NBIA cohort. This group, drawn from a population with high consanguinity and phenotypic variability, provides a unique opportunity for exploring genotype–phenotype correlations and regional iron patterns. Given the rarity of NBIA and the technical complexity of QSM acquisition and analysis, inclusion of a larger control group was not feasible. Nevertheless, we acknowledge this as a limitation.

Additionally, susceptibility artifacts and the exclusion of negative QSM values, while methodologically justified, may have introduced minor biases in iron quantification. Future studies could benefit from advanced artifact correction algorithms or incorporate negative QSM values through calibrated modeling to mitigate this potential bias.

5 | Conclusion

Our study highlights the value of QSM in the early diagnosis and monitoring of NBIA disorders, as it enables the detection of iron accumulation in regions that may be overlooked by conventional MRI. QSM proved to be a reliable and noninvasive biomarker for both detecting and quantifying iron burden. Among the brain regions evaluated, the GP consistently exhibited the highest susceptibility values across NBIA subtypes, reaffirming its significance in disease pathophysiology. Notably, the observed differences in iron deposition patterns, particularly the prominent GP involvement in classical PKAN and SN involvement in atypical PKAN, suggest potential subtype-specific mechanisms of iron dysregulation, which may have diagnostic and therapeutic implications.

Additionally, our findings highlight the importance of considering age-related susceptibility changes, as age emerged as a significant predictor of QSM values across multiple deep brain regions. The observation of reduced iron accumulation in the caudate and P, particularly among PKAN patients, may be relevant to the cognitive dysfunction frequently reported in NBIA syndromes, and warrants further investigation. Future research should aim to include larger cohorts, employ smaller voxel sizes, and incorporate comprehensive cognitive and motor assessments to refine our understanding of iron-related

neurodegeneration in NBIA. Longitudinal QSM studies, in particular, may offer critical insights into disease progression and aid in identifying potential therapeutic targets.

Author Contributions

Özge Uygun: data collection, clinical evaluation, patient recruitment, data analysis, and manuscript writing; Alpay Özcan and Fuat Kaan Aras: MRI acquisition and preprocessing, image segmentation, and QSM analysis; Evrim Bozdemir, Sibel Uğur İşeri, Nihan Hande Akçakaya, Orhan Mammadov, and Gülay Kır: Data analysis; Koray Kırımtay and Arzu Karabay: Genetic diagnosis; Murat Gültekin, Dilek İnce Günal, Neşe Tuncer, Fatma Betül Özdzilek, Banu Özen Barut, Ercan Köse, Hülya Apaydın, Asuman Ali, Sultan Çağırıcı, and Pınar Topaloğlu: patient recruitment; Alp Dinçer: data analysis, patient recruitment, study design; Zuhâl Yapıcı (supervisor): data collection, clinical evaluation, patient recruitment, data analysis, manuscript writing, supervision, and final manuscript revision for intellectual content.

Acknowledgments

We would like to thank Acibadem Altunizade Hospital Radiology Department for obtaining radiological data of the patients.

Ethics Statement

The study protocol was approved by the local ethics committee of Istanbul University, Istanbul Faculty of Medicine (2017/658).

Consent

The written informed consent was obtained from all participants.

Conflicts of Interest

The authors declare no conflicts of interest.

Data Availability Statement

Data available on request from the authors.

References

1. A. Gregory and S. J. Hayflick, "Neurodegeneration With Brain Iron Accumulation," *Folia Neuropathologica* 43, no. 4 (2005): 286–296.
2. H. Kolarova, J. Tan, T. M. Strom, T. Meitinger, M. Wagner, and T. Klopstock, "Lifetime Risk of Autosomal Recessive Neurodegeneration With Brain Iron Accumulation (NBIA) Disorders Calculated From Genetic Databases," *eBioMedicine* 77 (2022): 103869, <https://doi.org/10.1016/j.ebiom.2022.103869>.
3. S. J. Hayflick, M. A. Kurian, and P. Hogarth, "Neurodegeneration With Brain Iron Accumulation," *Handbook of Clinical Neurology* 147 (2018): 293–305, <https://doi.org/10.1016/B978-0-444-63233-3.00019-1>.
4. B. Zhou, S. K. Westaway, B. Levinson, M. A. Johnson, J. Gitschier, and S. J. Hayflick, "A Novel Pantothenate Kinase Gene (PANK2) Is Defective in Hallervorden-Spatz Syndrome," *Nature Genetics* 28, no. 4 (2001): 345–349, <https://doi.org/10.1038/ng572>.
5. S. J. Hayflick, "Unraveling the Hallervorden-Spatz Syndrome: Pantothenate Kinase-Associated Neurodegeneration Is the Name," *Current Opinion in Pediatrics* 15, no. 6 (2003): 572–577, <https://doi.org/10.1097/00008480-200312000-00005>.
6. N. V. Morgan, S. K. Westaway, J. E. Morton, et al., "PLA2G6, Encoding a Phospholipase A2, Is Mutated in Neurodegenerative Disorders With High Brain Iron," *Nature Genetics* 38, no. 7 (2006): 752–754, Epub 2006 Jun 18. Erratum in: *Nature Genetics*. 2006 Aug;38(8):957.

7. M. B. Hartig, A. Iuso, T. Haack, et al., "Absence of an Orphan Mitochondrial Protein, c19orf12, Causes a Distinct Subtype of Neurodegeneration With Brain Iron Accumulation," *American Journal of Human Genetics* 89, no. 4 (2011): 543–550, <https://doi.org/10.1016/j.ajhg.2011.09.007>.
8. T. B. Haack, P. Hogarth, M. C. Kruer, et al., "Exome Sequencing Reveals de Novo WDR45 Mutations Causing a Phenotypically Distinct, X-Linked Dominant Form of NBIA," *American Journal of Human Genetics* 91, no. 6 (2012): 1144–1149, <https://doi.org/10.1016/j.ajhg.2012.10.019>.
9. S. Choayb, H. Adil, D. Ali Mohamed, N. Allali, L. Chat, and S. El Haddad, "Eye of the Tiger Sign in Pantothenate Kinase-Associated Neurodegeneration," *Case Reports in Radiology* 7, no. 2021 (2021): 6633217, <https://doi.org/10.1155/2021/6633217>.
10. M. C. Kruer, N. Boddaert, S. A. Schneider, et al., "Neuroimaging Features of Neurodegeneration With Brain Iron Accumulation," *AJNR. American Journal of Neuroradiology* 33, no. 3 (2012): 407–414, <https://doi.org/10.3174/ajnr.A2677>.
11. P. Dusek, R. Mекle, M. Skowronska, et al., "Brain Iron and Metabolic Abnormalities in C19orf12 Mutation Carriers: A 7.0 Tesla MRI Study in Mitochondrial Membrane Protein-Associated Neurodegeneration," *Movement Disorders* 35, no. 1 (2020): 142–150, <https://doi.org/10.1002/mds.27827>.
12. Y. Kimura, N. Sato, A. Ishiyama, et al., "Serial MRI Alterations of Pediatric Patients With Beta-Propeller Protein Associated Neurodegeneration (BPAN)," *Journal of Neuroradiology* 48, no. 2 (2021): 88–93, <https://doi.org/10.1016/j.neurad.2020.04.002>.
13. M. McAuliffe, F. Lalonde, D. P. McGarry, W. Gandler, K. Csaky, and B. Trus, "Medical Image Processing, Analysis and Visualization in Clinical Research," *14th IEEE Symposium on Computer-Based Medical Systems* 14 (2001): 381–386, <https://doi.org/10.1109/CBMS.2001.941749>.
14. W. Li, B. Wu, and L. Chunlei, "STI Suite: A Software Package for Quantitative Susceptibility Imaging," *Proceedings on International Society for Magnetic Resonance in Medicine*, 22, (2014).
15. B. Wu, W. Li, A. Guidon, and C. Liu, "Whole Brain Susceptibility Mapping Using Compressed Sensing," *Magnetic Resonance in Medicine* 67, no. 1 (2012): 137–147, <https://doi.org/10.1002/mrm.23000>.
16. W. Li, A. V. Avram, B. Wu, X. Xiao, and C. Liu, "Integrated Laplacian-Based Phase Unwrapping and Background Phase Removal for Quantitative Susceptibility Mapping," *NMR in Biomedicine* 27, no. 2 (2014): 219–227, <https://doi.org/10.1002/nbm.3056>.
17. A. Ozcan, O. Uygun, F. K. Aras, et al., "QSM Attributes of Neurodegeneration With Brain Iron Accumulation Disorders Subtypes in Basal Ganglia," 28th Joint Annual Meeting ISMRM-ESMRB, Sydney, Australia, (2020).
18. I. Hinarejos, C. Machuca-Arellano, P. Sancho, and C. Espinós, "Mitochondrial Dysfunction, Oxidative Stress and Neuroinflammation in Neurodegeneration With Brain Iron Accumulation (NBIA)," *Antioxidants* 9, no. 10 (2020): 1020, <https://doi.org/10.3390/antiox9101020>.
19. L. Zecca, M. B. Youdim, P. Riederer, J. R. Connor, and R. R. Crichton, "Iron, Brain Ageing and Neurodegenerative Disorders," *Nature Reviews. Neuroscience* 5, no. 11 (2004): 863–873, <https://doi.org/10.1038/nrn1537>.
20. N. C. Andrews, "Iron Homeostasis: Insights From Genetics and Animal Models," *Nature Reviews. Genetics* 1, no. 3 (2000): 208–217, <https://doi.org/10.1038/35042073>.
21. N. C. Andrews, "Disorders of Iron Metabolism," *New England Journal of Medicine* 341, no. 26 (1999): 1986–1995, Erratum in: *N Engl J Med* 2000 Feb 3;342(5):364.
22. A. Carocci, A. Catalano, M. S. Sinicropi, and G. Genchi, "Oxidative Stress and Neurodegeneration: The Involvement of Iron," *Biometals* 31, no. 5 (2018): 715–735, <https://doi.org/10.1007/s10534-018-0126-2>.
23. S. Hametner, I. Wimmer, L. Haider, S. Pfeifenbring, W. Brück, and H. Lassmann, "Iron and Neurodegeneration in the Multiple Sclerosis

- Brain," *Annals of Neurology* 74, no. 6 (2013): 848–861, <https://doi.org/10.1002/ana.23974>.
24. L. Mezzaroba, D. F. Alfieri, A. N. Colado Simão, and E. M. Vissoci Reiche, "The Role of Zinc, Copper, Manganese and Iron in Neurodegenerative Diseases," *Neurotoxicology* 74 (2019): 230–241, <https://doi.org/10.1016/j.neuro.2019.07.007>.
25. J. Pujol, C. Junqué, P. Vendrell, et al., "Biological Significance of Iron-Related Magnetic Resonance Imaging Changes in the Brain," *Archives of Neurology* 49, no. 7 (1992): 711–717, <https://doi.org/10.1001/archneur.1992.00530310053012>.
26. S. D. Brass, N. K. Chen, R. V. Mulkern, and R. Bakshi, "Magnetic Resonance Imaging of Iron Deposition in Neurological Disorders," *Topics in Magnetic Resonance Imaging* 17, no. 1 (2006): 31–40, <https://doi.org/10.1097/01.rmr.0000245459.82782.e4>.
27. J. F. Schenck, "The Role of Magnetic Susceptibility in Magnetic Resonance Imaging: MRI Magnetic Compatibility of the First and Second Kinds," *Medical Physics* 23, no. 6 (1996): 815–850, <https://doi.org/10.1118/1.597854>.
28. J. R. Reichenbach, R. Venkatesan, D. J. Schillinger, D. K. Kido, and E. M. Haacke, "Small Vessels in the Human Brain: MR Venography With Deoxyhemoglobin as an Intrinsic Contrast Agent," *Radiology* 204, no. 1 (1997): 272–277, <https://doi.org/10.1148/radiology.204.1.9205259>.
29. N. Şahin, A. Solak, B. Genç, and N. Bilgiç, "Susceptibility-Weighted MR Imaging: Added Value of Susceptibility Signals in Diagnosis of Hemorrhagic Lesions of the Brain," *Turkish Journal of Cerebrovascular Diseases* 20, no. 3 (2014): 77–86.
30. E. M. Haacke, Y. Xu, Y. C. Cheng, and J. R. Reichenbach, "Susceptibility Weighted Imaging (SWI)," *Magnetic Resonance in Medicine* 52, no. 3 (2004): 612–618, <https://doi.org/10.1002/mrm.20198>.
31. L. de Rochefort, R. Brown, M. R. Prince, and Y. Wang, "Quantitative MR Susceptibility Mapping Using Piece-Wise Constant Regularized Inversion of the Magnetic Field," *Magnetic Resonance in Medicine* 60, no. 4 (2008): 1003–1009, <https://doi.org/10.1002/mrm.21710>.
32. W. Zheng, H. Nichol, S. Liu, Y. C. Cheng, and E. M. Haacke, "Measuring Iron in the Brain Using Quantitative Susceptibility Mapping and X-Ray Fluorescence Imaging," *NeuroImage* 78 (2013): 68–74, <https://doi.org/10.1016/j.neuroimage.2013.04.022>.
33. C. Liu, H. Wei, N. J. Gong, M. Cronin, R. Dibb, and K. Decker, "Quantitative Susceptibility Mapping: Contrast Mechanisms and Clinical Applications," *Tomography* 1, no. 1 (2015): 3–17, <https://doi.org/10.18383/j.tom.2015.00136>.
34. C. Stüber, D. Pitt, and Y. Wang, "Iron in Multiple Sclerosis and Its Noninvasive Imaging With Quantitative Susceptibility Mapping," *International Journal of Molecular Sciences* 17, no. 1 (2016): 100, <https://doi.org/10.3390/ijms17010100>.
35. J. R. Reichenbach, "The Future of Susceptibility Contrast for Assessment of Anatomy and Function," *NeuroImage* 62, no. 2 (2012): 1311–1315, <https://doi.org/10.1016/j.neuroimage.2012.01.004>.
36. C. Langkammer, T. Liu, M. Khalil, et al., "Quantitative Susceptibility Mapping in Multiple Sclerosis," *Radiology* 267, no. 2 (2013): 551–559, <https://doi.org/10.1148/radiol.12120707>.
37. H. G. Kim, S. Park, H. Y. Rhee, et al., "Quantitative Susceptibility Mapping to Evaluate the Early Stage of Alzheimer's Disease," *NeuroImage: Clinical* 24, no. 16 (2017): 429–438, <https://doi.org/10.1016/j.nicl.2017.08.019>.
38. J. H. Barbosa, A. C. Santos, V. Tumas, et al., "Quantifying Brain Iron Deposition in Patients With Parkinson's Disease Using Quantitative Susceptibility Mapping, R2 and R2'," *Magnetic Resonance Imaging* 33, no. 5 (2015): 559–565, <https://doi.org/10.1016/j.mri.2015.02.021>.
39. S. Ropele and C. Langkammer, "Iron Quantification With Susceptibility," *NMR in Biomedicine* 30, no. 4 (2017): 3534, <https://doi.org/10.1002/nbm.3534>.
40. J. H. Duyn and J. Schenck, "Contributions to Magnetic Susceptibility of Brain Tissue," *NMR in Biomedicine* 30, no. 4 (2017): 3546, <https://doi.org/10.1002/nbm.3546>.
41. P. Dusek, E. M. Tovar Martinez, V. I. Madai, et al., "7-Tesla Magnetic Resonance Imaging for Brain Iron Quantification in Homozygous and Heterozygous PANK2 Mutation Carriers," *Movement Disorders Clinical Practice* 1, no. 4 (2014): 329–335, <https://doi.org/10.1002/mdc3.12080>.
42. F. Darki, F. Nemmi, A. Möller, R. Sitnikov, and T. Klingberg, "Quantitative Susceptibility Mapping of Striatum in Children and Adults, and Its Association With Working Memory Performance," *NeuroImage* 1, no. 136 (2016): 208–214, <https://doi.org/10.1016/j.neuroimage.2016.04.065>.
43. A. M. Daugherty and N. Raz, "Appraising the Role of Iron in Brain Aging and Cognition: Promises and Limitations of MRI Methods," *Neuropsychology Review* 25, no. 3 (2015): 272–287, Erratum in: *Neuropsychology Review*. 2015 Sep;25(3):288.
44. W. Li, C. Langkammer, Y. H. Chou, et al., "Association Between Increased Magnetic Susceptibility of Deep Gray Matter Nuclei and Decreased Motor Function in Healthy Adults," *NeuroImage* 105 (2015): 45–52, <https://doi.org/10.1016/j.neuroimage.2014.10.009>.
45. U. Löbel, F. Schweser, M. Nickel, et al., "Brain Iron Quantification by MRI in Mitochondrial Membrane Protein-Associated Neurodegeneration Under Iron-Chelating Therapy," *Annals of Clinical Translational Neurology* 1, no. 12 (2014): 1041–1046, <https://doi.org/10.1002/acn3.116>.
46. T. Fujiwara, Y. Watanabe, H. Tanaka, et al., "Quantitative Susceptibility Mapping (QSM) Evaluation of Infantile Neuroaxonal Dystrophy," *BJR Case Reports* 5, no. 2 (2019): 20180078, <https://doi.org/10.1259/bjrcr.20180078>.
47. A. Ishiyama, Y. Kimura, A. Iida, et al., "Transient Swelling in the Globus Pallidus and Substantia Nigra in Childhood Suggests SENDA/BPAN," *Neurology* 90, no. 21 (2018): 974–976, <https://doi.org/10.1212/WNL.0000000000005564>.
48. K. Kırımtay, B. Temizci, M. Gültekin, Z. Yapıcı, and A. Karabay, "Novel Mutations in ATP13A2 Associated With Mixed Neurological Presentations and Iron Toxicity due to Nonsense-Mediated Decay," *Brain Research* 1750 (2021): 147167, <https://doi.org/10.1016/j.brainres.2020.147167>.